Available online at www.sciencedirect.com
ScienceDirect
Engineering Geology 88 (2006) 23–40
ENGINEERING GEOLOGY
www.elsevier.com/locate/enggeo

On the evaluation of unsaturated flow in a natural slope in Rio de Janeiro, Brazil

D.M.S. Gerscovich [a,*], E.A. Vargas [b], T.M.P. de Campos [b]

[a] *Structure and Foundation Department, State University of Rio de Janeiro, Rua São Francisco Xavier 525/5018-A, Maracanã, 20550-013, Rio de Janeiro, RJ, Brazil*

[b] *Civil Engineering Department, Catholic University of Rio de Janeiro, Rua Marquês de São Vicente 225/301-L, Gávea, 22453-900, Rio de Janeiro, RJ, Brazil*

Received 8 July 2005; received in revised form 13 July 2006; accepted 17 July 2006

Abstract

Geotechnical engineers and geologists are frequently concerned with the complex phenomenon of rainstorm-induced landslides in mountainous tropical regions. This paper analyses the hydrological conditions that contributed to a huge deep-seated slide of a slope in Rio de Janeiro, Brazil. The slope failure occurred after a short period of intense rainfall, buried cars, and caused structural damages to an adjacent building. On the following day, the failure surface was completely saturated, despite the fact that no groundwater was observed within the slope. Understanding a rain-induced landslide is a considerable challenge. In the present case, there was an extra question to be answered: why were no slope movements observed a few months earlier, when a more intense rainfall reached the slope? Geological and geotechnical surveys were carried out aiming at determining complete soil profile characterization, piezometric levels and hydraulic parameters. Field investigations indicated a variable thickness unsaturated residual soil layer overlying a gneissic rock. The transition between the saprolitic soil and the sound rock consisted of a highly fractured and weathered rock. 3D flow modelling has shown that the amount of rain infiltration was insufficient to produce positive pore-water pressures. It was likely that development of preferential infiltration paths could explain the hydrological conditions of the slope during landslide. Water infiltration through the fractured soil–rock transition induced a rapid development of positive pore water within the soil mass. This favourable scenario might have been created by the lack of maintenance of the crest drainage channel, adjacent to the slide area. It is a common engineering practice to try to associate rainfall amounts to the risk of slope failure. The role that bedrock plays in generating pore pressure is seldom considered. The numerical analyses presented in this paper pointed out at the complexity of flow modeling of rain infiltration through unsaturated residual soil slopes. It essentially revealed that flow mechanisms other than rain infiltration over the slope surface might play a major role on hydrological pattern of slopes.

Keywords: Unsaturated soil; Residual soil; Rainfall; Landslides; Numerical modeling; Transient flow

1. Introduction

The role of rainfall infiltration in triggering landslides in tropical regions is being a challenge for geotechnical engineers and engineering geologists. Many authors have attempted to address the likely causes of these failures

* Corresponding author.
E-mail address: deniseg@uerj.br (D.M.S. Gerscovich).

0013-7952/$ - see front matter © 2006 Published by Elsevier B.V.
doi:10.1016/j.enggeo.2006.07.008

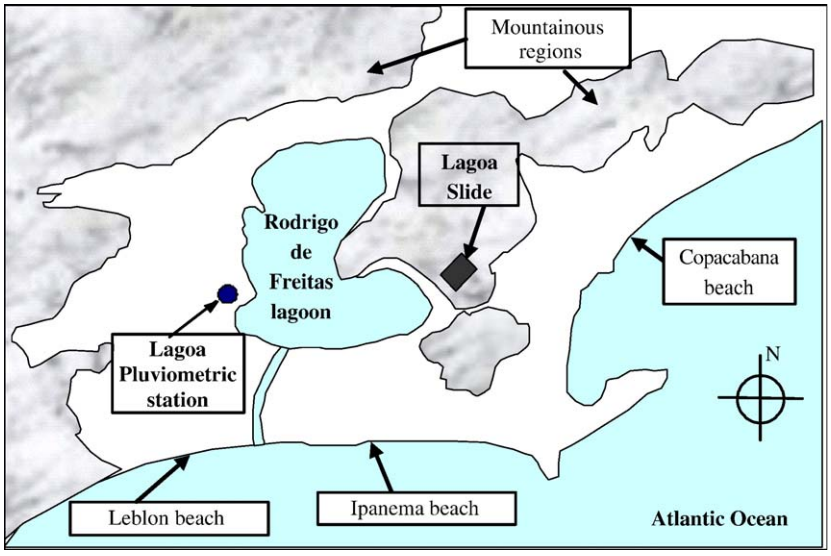

Fig. 1. Rio de Janeiro map.

(e.g., Costa Nunes et al., 1989; Wolle and Hachich, 1989; Au, 1998; Kim et al., 2004). Some of them have also tried to define rainfall thresholds for landslides, which are generally expressed as a function of rainfall intensity and duration (e.g., Vargas, 1971; Lumb, 1975; Brand, 1984).

Due to geological, geotechnical and geomorphological uncertainties, it is usually very difficult to predict where and when a landslide may occur by the current state of the art. Nevertheless, it is generally recognized that rainfall-induced landslides are caused by changes in pore-water pressures. The increase in pore pressure decreases soil effective stress and, thus, reduces soil shear strength. Further studies have illustrated that in some cases of rainfall-induced landslides, movement along the sliding surface leads to crushing of the soil grains, which results in liquefaction along this surface, finally resulting in rapid movements and long run out distances (e.g., Wang and Sassa, 2003).

Rain-induced soil and/or rock mass movements, sometimes of catastrophic consequences, occur repeatedly in the city of Rio de Janeiro and other mountainous areas in the state. These movements may occur in either natural or man-induced slopes, during or immediately after rainfall events.

The state of Rio de Janeiro is located in the southeastern region of Brazil. Its geomorphology exhibits a succession of coastal plains and valleys separated by three main mountain chains. The mountainous relief has elevations ranging from sea level to slightly over 1000 m.

The capital of Rio de Janeiro state, also called Rio de Janeiro, has a tropical humid climate, with a hot rainy summer season and a mild and relatively dry winter. The mean annual temperature is high, above 22 °C, with mean daily summer temperature ranging from 30 °C to

Fig. 2. Day after photo of Lagoa landslide.

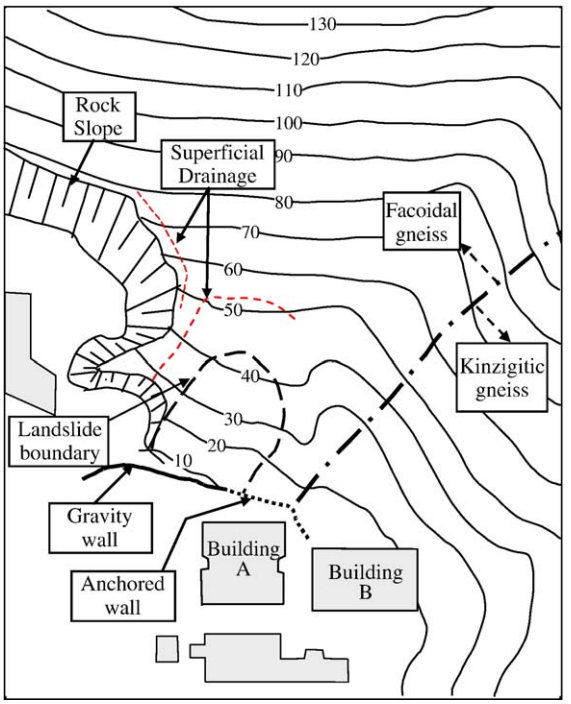

Fig. 3. Schematic site plan before landslide.

32 °C, with peak values over 40 °C. During the winter, the monthly temperatures are in excess of 18 °C. Therefore, relatively deep soil profiles can be found on hillslopes. The weathering mechanism is mainly attributed to chemical processes.

Landslides, which occurred in the city of Rio de Janeiro and nearby mountain chains during the summer of 1976 and 1967, are examples of catastrophic mass movements, as a result of intense rainfalls (Costa Nunes et al., 1979). In this period, almost 2700 lives were lost. The damage to property and the resulting effects on industry were inestimable (Jones, 1973). In the summer of 1981 and 1982, a major landslide in an important access highway in Rio de Janeiro caused the death of 14 people and, again, with huge financial loss. Since then, many other landslides occurred in the state of Rio de Janeiro.

In February 1988, a considerable number of soil/rock slides occurred in different slopes in Rio de Janeiro city. Most of them were shallow and small slides, but others were quite long in extension (100–150 m). These slides are amongst the largest that have occurred in the city. In a period of 21 days, the accumulated pluviometric record was 515.6 mm, with a rain peak of 85.4 mm in a single day.

Nine months later, in November 1988, a deep-seated slide occurred in a re-vegetated slope, adjacent to a relatively high-income class building. The slope is located next to Rodrigo de Freitas lagoon. As illustrated in Fig. 1, the lagoon is close to the well-known tourist spots of Copacabana and Ipanema in the city of Rio de Janeiro.

This paper describes the geological and geotechnical studies carried out in an attempt to understand the flow mechanism that triggered the landslide in November 1988. This landslide will be herein called the Lagoa slide.

2. Landslide description

On November 7, 1988, at 3:00 PM, 5000 m^3 of soil failed over a deep, spoon shaped, surface (Fig. 2). The failure caused serious structural and material damages to an adjacent building, with the shearing of one pillar and complete destruction of one apartment. Several cars in external and internal building parking areas were also damaged. Luckily the slide did not cause any loss of life.

On the following day and continuously for the following week after the slide there were indications of full saturation of the failure surface, with groundwater

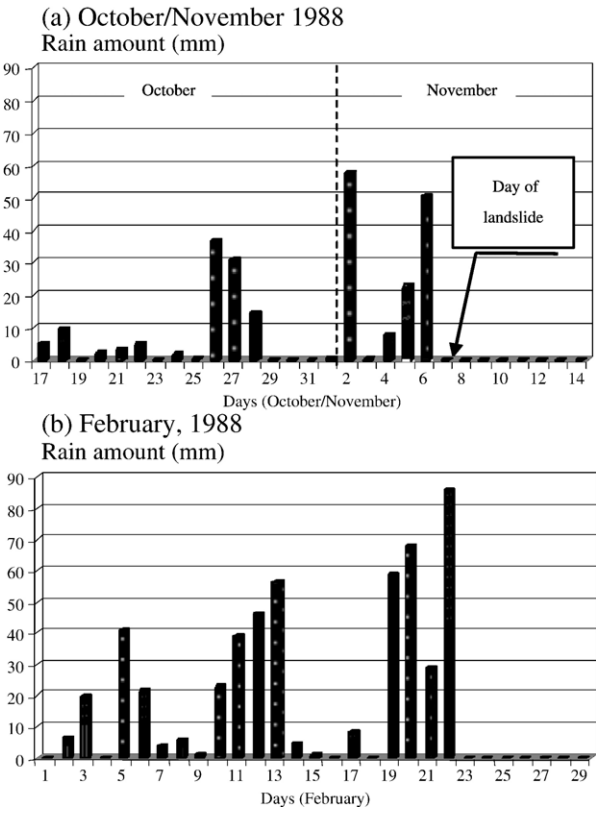

Fig. 4. Daily rain amount.

springs at its upper region. Full blockage of the crest channel, adjacent to the slide area, due to lack of maintenance of the superficial drainage system was also observed.

Fig. 3 shows a schematic plan of the site before the landslide. The slope summit has a maximum elevation of 384 m, and surface inclinations ranging from 30° to 55°. At the toe of the slope, there was a gravity wall aligned with an anchored wall, located at the rear of the Building A. A subsurface drainage system and a crest channel, located at the upper region of the slope, comprised previous slope stabilization measures.

In the past, low-income people occupied this area in a disorganized way, forming a so-called favela (slum). Removal of the vegetative cover and execution of cuts without any safety criteria is common practice in this kind of land occupation. In the beginning of the 1970s, these people were moved to other sites and the slope was progressively re-vegetated.

Daily pluviometric records, provided by the Lagoa monitoring station, located approximately 4 km from the slope, is presented in Fig. 4a. The accumulated rain amount from October 17 to November 7 (21 days) summed a total of 246.3 mm. The slope failure occurred when the rain had already ceased.

In February 1988, in the peak of the summer season, heavy rainfalls (Fig. 4b) induced a considerable number of soil/rock slides in different slopes in Rio de Janeiro city. As the accumulated rain registered in November was nearly half of that observed in February, it is apparent that the rain amount, by itself, would not explain the slope failure.

Preliminary analyses indicated that slope instability could have been caused either by obstruction of the internal drainage system of the gravity wall, located at the toe of the slope, or by rise of the water table due to rainfall infiltration. The hypothesis of failure of the retaining structure was unlikely, since the shape of the

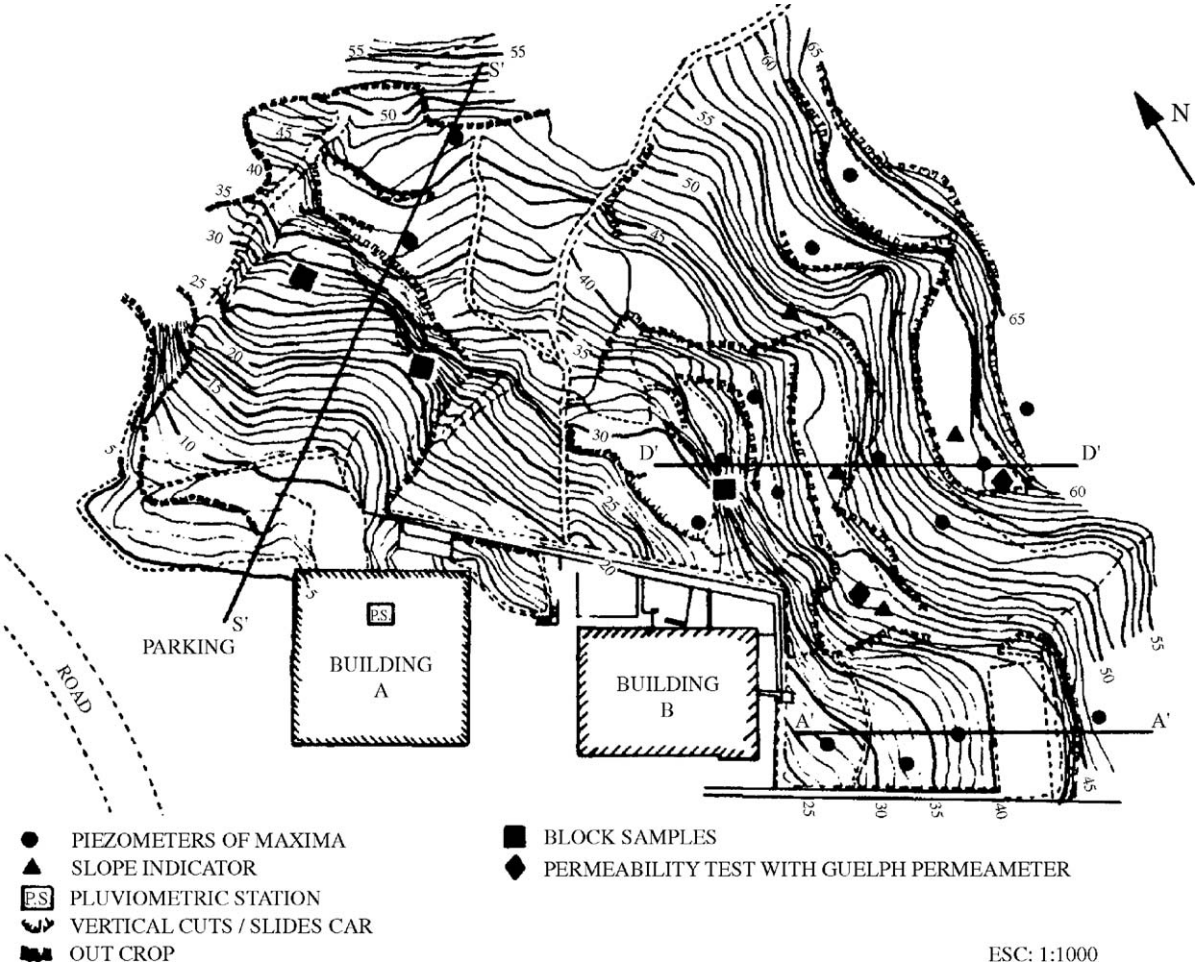

Fig. 5. Topographic plant and field instrumentation after landslide.

failure surface suggested that the soil movement predominantly occurred above the wall. In addition, there was no evidence that the accumulated rainfall could have raised the water table, which was located at a considerable depth below ground level. Furthermore, it is well known that water infiltration due to rainfall in an unsaturated soil induces a decrease in matric suction and promotes, usually, shallow slope failures (e.g., Kim et al., 2004). As just after the accident there were evidences that the failure surface would be fully saturated, a mechanism that could explain the deep-seated slope failure should be associated to major changes of the slope hydrogeology.

3. Geological and geotechnical surveys

A comprehensive series of field and laboratory tests were carried out to determine soil profile and geotechnical and hydrogeological parameters.

Field investigation comprised seismic refraction surveys, percussion and rotary drillings. They indicated a varying thickness layer of colluvial and/or young residual soil, overlying bedrock that outcropped at the upper and left sides of the landslide boundary.

Geologically, the slope is composed of a residual soil originated from a gneissic metamorphic rock. At the site, the rock structure is folded and exhibits a contact between two different types of gneiss: facoidal and kinzigitic (Fig. 3).

The facoidal gneiss was characterized by the presence of large feldspar crystals, with “egg shaped” ends, within a matrix composed of quartz, feldspar and biotite. The kinzigitic gneiss was constituted by thin layers rich in biotite, cordierite, quartz, sillimantite and granade, intercalated by layers of quartz of equivalent thickness.

The facoidal gneiss, normally less fractured and weathered, emerges at the upper part of the slope and dips bellow the kinzigitic gneiss with a dip angle higher than 60°. Both types of gneiss were crossed by two subvertical fracture systems and one relief jointing system. No regional faulting systems were identified in the area.

The overlying residual soil indicated depths varying from 0 m to 15 m. The weathering profile was composed of a superficial mature clayey sand residual soil, with an average thickness of 1 m, underlain by a layer of a sandy matrix young residual soil (saprolitic soil), with a well-defined inherited mineral alignment from the parent rock. The transition between the sound rock and the saprolitic soil is a highly fractured and weathered rock with a thickness varying within 4–10 m.

The mechanical soundings did not indicate the presence of a groundwater level within the soil mass. However, water level was observed in some rotary drillings within the fractured rock layer.

3.1. Field instrumentation and testing

Field instrumentation was installed outside the slide area, in order to avoid interference of recovery works, which started soon after the accident. Twenty-one holes were drilled for the installation of fifteen piezometers and six slope indicators (Fig. 5). A pluviometric station was also installed on the roof of Building A. Fig. 6 shows soil profiles of the instrumented area.

Maxima piezometers were installed at the soil–rock interface to record maximum transient water pressure levels. These piezometers are similar to the bucket type piezometer developed in Hong Kong (Brand, 1985). They consisted of a rigid PVC tube with a porous tip (Casagrande piezometer) and a segmented plastic tube positioned inside the PVC tube. The upper part of each segment is perforated and adjacent segments are linked through small pieces of aluminium rod. The bottom end of the plastic tube is sealed. The plastic tube can be removed for inspection and then replaced, assuring a constant elevation for each segment during the monitoring period. The maximum pressure head is measured

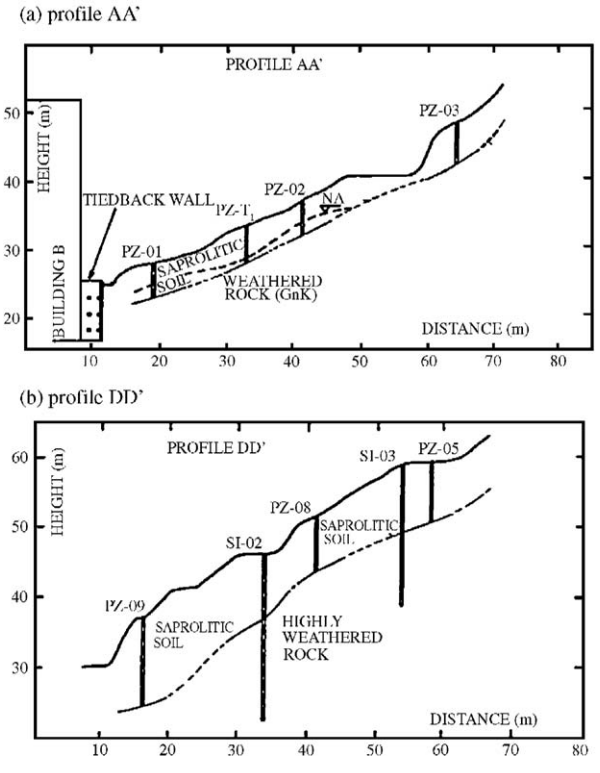

Fig. 6. Soil profiles of the instrumented area.

independently of the day of reading by identifying the upper limit of filled segments.

Perforated plastic tubes were also installed inside the inclinometer tubes. From the 15 piezometers and 6 water level indicators installed, positioned far from the sliding area, only three indicated the occurrence of a localized water level within the soil slope.

Results of more than 3 years of monitoring indicated that water levels were confined to a small area, always restricted to the region of fractured rock. This probably was due to a low efficiency of relatively old horizontal drains installed at the site. No slope movements were detected during the monitoring period.

The hydraulic conductivity (k) profile of the residual soil was obtained by means of Guelph permeameter tests (Reynolds and Elrick, 1987) in two positions, at the top and at the base of the slope, behind Building B (Fig. 5). The tests were performed at 6 different depths between 0.42 and 3.17 m.

Guelph permeameter test assumes that flow through an unsaturated soil rapidly achieves a steady-state regime when a small constant head is imposed. Besides, test interpretation considers the relationship between hydraulic conductivity (k) and matric soil suction according to Gardner's proposition (Gardner, 1958):

$$k = k_{sat} e^{\alpha\psi} \quad (1)$$

where, k_{sat} is the saturated hydraulic conductivity (m/s); ψ is the matric suction (m H_2O) and α is a fitting equation parameter (m^{-1}), that may be related to capillary properties of the soil. Both k_{sat} and α are computed by applying different constant pressure heads inside the permeameter and measuring flux.

Guelph test results, presented in Fig. 7, indicate a 1.5-m-deep layer of low hydraulic conductivity. A more intense weathering process in this layer produces higher percentage of clay particles. In the underlying soil profile, the saturated hydraulic conductivity tends to increase. The values of the equation parameter (α) varied between 1 and 62 m^{-1} according to the percentage of clay fraction. lower α values are expected for coarse to fine sands and greater values for fine-grained soils (Elrick et al., 1989).

The saturated hydraulic conductivity (k_{sat}) profiles also revealed significant differences between tests carried out at the top and base of the slope. Lower values of hydraulic conductivity at the base of slopes have also been reported elsewhere (Vaughan, 1985; Reid et al., 1988). This rather accentuated variability in hydraulic conductivity produces non-uniform flow paths and, therefore, non-uniform distribution of pore-water pressure. Gerscovich et al. (2004) analysed infiltration processes due to water ponding at ground surface and showed that even small contrasts of k_{sat} produces strong differences on pore-water pressure distributions in unsaturated soils.

The major difference between flow processes in saturated and unsaturated soils is the magnitude of the hydraulic conductivity. The transition from a saturated to an unsaturated condition reduces the hydraulic conductivity by several orders of magnitude in relation to its

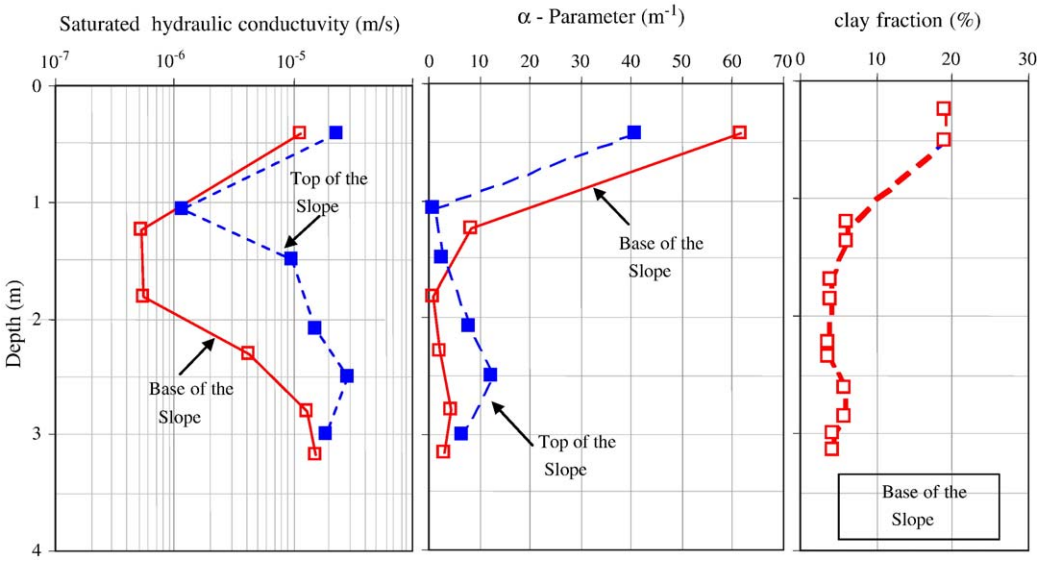

Fig. 7. Hydraulic conductivity parameters provided by Guelph permeameter tests and clay fraction profile at the base of the slope.

saturated value, even at low matric suction levels. In a drying process, the larger pores, which have large influence on the saturated hydraulic conductivity value, become empty before flow paths are transferred to the smaller pores. Also, the water that remains in the pores may be held against the particle surface in the form of menisci, forming discontinuous channels (Hillel, 1971).

3.2. Laboratory investigation

Besides tests to obtain unsaturated soil shear strength parameters, not taken into account in the context of the present work, the laboratory work comprised soil characterization and tests to determine the relationships among hydraulic conductivity, soil suction and soil moisture. The relationship between the soil–water content and matric suction is conventionally referred to as the soil–water characteristic curve (SWCC) or the soil–water retention curve (SWRC).

Block samples were extracted at the slope failure surface and at a trench 50 m away from the failure zone, behind Building B (Fig. 5). Two different materials appeared at the failure surface: an apparently homogeneous and isotropic red-coloured mature residual soil, and a grey saprolitic soil, with a well-defined mineral alignment. At the trench, only the saprolitic soil was extracted. Table 1 shows a summary of the characterization tests and average physical indexes. The saprolitic soil from the trench was coarser and denser than the one from the slip surface.

The volumetric soil moisture profile of the saprolitic soil extracted from the trench, located behind Building B, is shown in Fig. 8. The results indicated a volumetric water content around 25% on the surface and a gradual reduction with depth. Below 2 m depth, this value is approximately constant and equal to 9%.

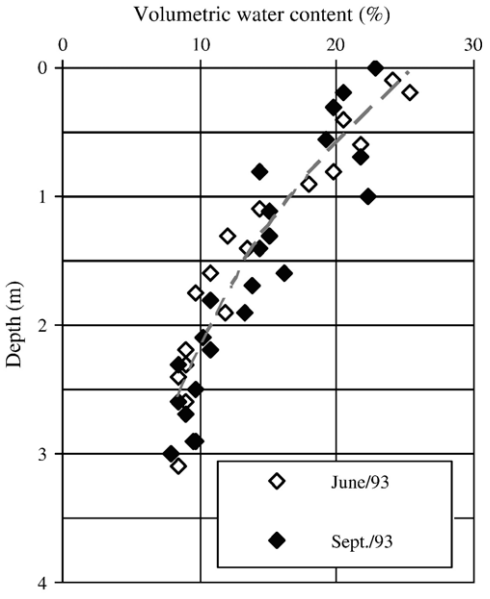

Fig. 8. Volumetric water content profiles of the saprolitic soil from the trench.

Soil–water retention curves (SWRC) were obtained using a suction plate device. The tests were performed on the saprolitic soil samples from the slip surface, following drying and wetting paths. The results, shown in Fig. 9, indicate a small deviation between the wetting and drying curves. Water contents of wetting curves are usually lower than the corresponding values of drying

Table 1
Soil characterization

Location	Slip surface		Trench
Soil type	Saprolitic soil	Mature residual soil	Saprolitic soil
Sand (%)	63.0	56.0	82.0
Silt (%)	27.5	34.0	9.8
Clay (%)	9.5	10.0	8.2
ω_L (%)	38.2	39.5	–
ω_P (%)	NP	24.7	–
ω (%)	19.0	21.2	6.4
θ (%)	22.4	25.5	10.3
G_s	2.64	2.63	2.66
e	1.19	1.14	0.62
n	0.54	0.53	0.38
γ_t (kN/m^3)	14.0	14.6	17.1

ω_L=liquid limit; ω_L=plasticity limit; ω=water content; θ=volumetric water content; G_s=specific gravity of grains; e=voids ratio, n=porosity, γ_t=in situ density.

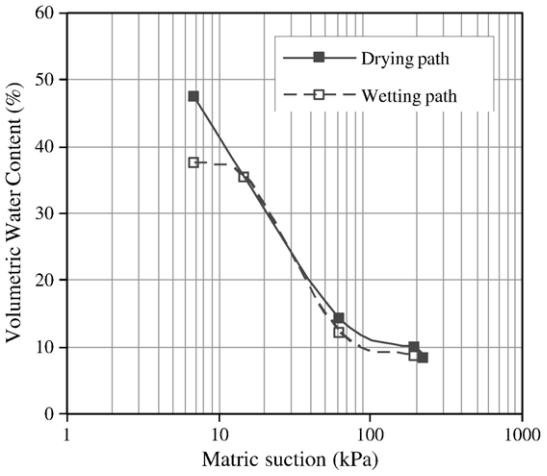

Fig. 9. Soil–water retention curve of the saprolitic soil from the slip surface.

curves, at any suction value. Besides, full saturation condition is rarely achieved in wetting processes. This hysteretic pattern is mainly attributed to geometric non-uniformities of interconnected pores and/or to entrapped air. Changes in soil structure due to swelling or shrinking phenomena is also partially responsible for this response (Hillel, 1971; Vanapalli et al., 1999). In the present case, the residual soils did not show any relevant volume change when submitted to wet/dry processes from their natural moisture content condition.

Soil characterization of the saprolitic soil of the slip surface (Table 1) indicates that the saturated volumetric water content ($\theta_s = n \times S$) is equal to 54%. However, the SWRC, obtained in the wetting process (Fig. 9), suggests a lower value, around 40%. This deviation is mainly attributed to entrapped air effects.

The bubbling pressure (ψ_b), which defines the soil suction at which the water in the largest pores starts to drain, is less than 15 kPa and is in agreement to the range experimentally observed in Brazilian residual soils (e.g., Gerscovich and Sayão, 2002). A range of $\psi_b = 0.2–7.5$ kPa for coarse to fine sands, $\psi_b = 7–25$ kPa for silty soils, and $\psi_b > 25$ kPa for clays is expected (Aubertin et al., 1998).

The experimental results (Fig. 9) indicated a residual suction (ψ_r) greater than 100 kPa. This residual suction (ψ_r) corresponds to a lower limit beyond which an increase in matric suction does not reduce significantly the soil water content. van Genuchten (1980) has suggested $\psi_r = 1500$ kPa as a reasonable assumption. In the present study, ψ_r was considered equal to 10^4 kPa. This value was adopted to describe the SWRC of other Brazilian residual soils and showed to be adequate (Gerscovich and Sayão, 2002).

A number of equations are available in the literature to mathematically represent the SWRC data. Some equations are based on the assumption that the curve shape is dependent upon pore size distribution (e.g., Gardner, 1958; Brooks and Corey, 1964; van Genuchten, 1980; Fredlund and Xing, 1994). Others assume that the SWRC can be directly estimated from the grain size distribution and physical properties of soils (e.g., Gosh, 1980; Rawls and Brakensiek, 1989). The suitability of different SWRC equations was evaluated and those proposed by Gardner, van Genuchten, and Fredlund and Xing provided best fits to the experimental data. Gardner equation requires two equation parameters (*a* and *n*). The proposition by van Genuchten is similar to the previous one but includes a third parameter (*m*). Fredlund and Xing equation primarily considers the drying curve and requires three equation parameters (*a*, *m* and *n*). In the present analysis, an optimization method, based on genetic algorithms, was used to search for the optimum parameters and minimum errors (Gerscovich et al., 2004). The quality of the curve fitting was measured by an error criterion (ε) defined by the following equation:

$$\varepsilon = \frac{\sqrt{\sum(\theta_i - \hat{\theta}_i)^2}}{\sqrt{\sum(\hat{\theta}_i)^2}} \tag{2}$$

where θ_i and $\hat{\theta}_i$ are, respectively, the predicted and measured volumetric water contents. The proposed error criterion normalizes the commonly used root mean square error (RMSQ), eliminating the influence of the order of magnitude of the experimental values. Gardner, van Genuchten and Fredlund and Xing equation parameters are shown in Table 2, as well as the computed errors obtained.

Saturated hydraulic conductivity laboratory tests were carried out on 100-mm-diameter samples of saprolitic soil, extracted from the trench. The results (Fig. 10a) indicated a slight reduction from 6×10^{-6} to 2×10^{-6} m/s with increase in effective stress. The saturated hydraulic conductivity obtained in the field by Guelph permeameter tests showed a greater deviation that may be attributed to field heterogeneities. The relationship between the saturated hydraulic conductivity and void ratio is also presented in Fig. 10b. The results revealed a reasonable alignment and a major importance of soil structure on the hydraulic conductivity of residual soils.

4. Numerical modeling

The general flow equation that controls steady–unsteady state flow problems through a 2-D, 3-D saturated–unsaturated porous media, usually referred to as Richards equation, can be written as

$$\frac{\partial}{\partial \chi_i}\left[k_{ij}^s K_r \frac{\partial h_p}{\partial \chi_j} + k_{i2}^s K_r\right] = \left[C(\psi) + \frac{\theta(\psi)}{n} S_s\right] \frac{\partial h_p}{\partial t} \tag{3}$$

where, h_p is the pressure head, ψ is the matric suction, θ is the volumetric water content, k_{ij}^s is the hydraulic conductivity tensor at saturation; K_r is the

Table 2
SWRC fitted parameters and computed errors

Equation	Parameters			Computed error
	a	*n*	*m*	
Gardner (1958)	0.01	1.53	–	0.0084
van Genuchten (1980)	0.01	1.53	0.99	0.0086
Fredlund and Xing (1994)	49.04 (kPa)	1.3	3.62	0.0089

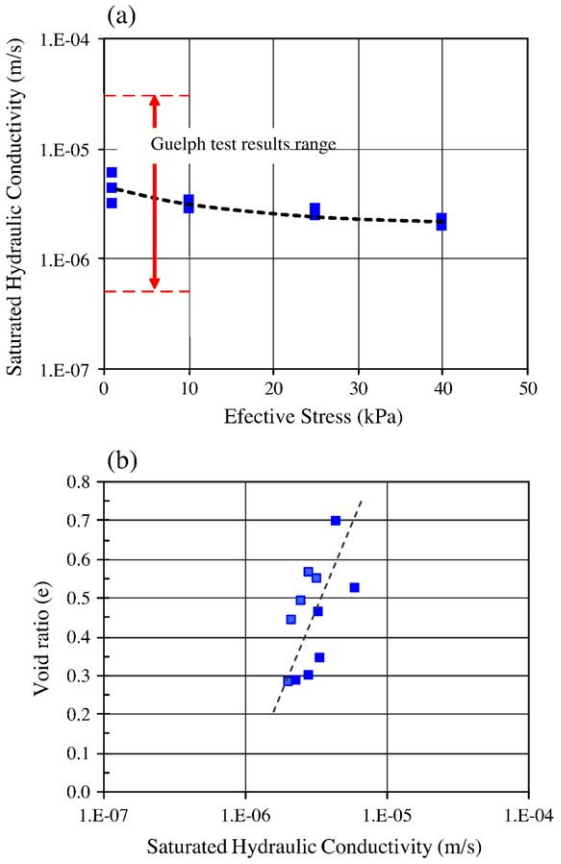

Fig. 10. Saturated hydraulic conductivity of the saprolitic soil from the trench.

relative hydraulic conductivity, which is defined as the relationship between unsaturated and saturated hydraulic conductivities (k/k_{sat}); K_r varies between 0 and 1 and is a scalar function of the degree of saturation ($K_r(S)$); $C(\psi)$ is the volumetric water retention capacity ($\partial\theta/\partial\psi$), given by the tangent to the SWCC, n is the porosity and S_s is the coefficient of specific storage. S_s physically represents the volume of water that a unit volume of porous media releases from storage under a unit decline in hydraulic head (Freeze and Cherry, 1979). The flow equation is highly nonlinear in the unsaturated zone, since coefficients $K_r(\psi)$ and $C(\psi)$ are functions of the independent variable ψ.

4.1. FLOW3D computer program

The numerical modelling was carried out using the computer program FLOW3D (Gerscovich, 1994). The program uses the finite element method for solving Eq. (3). The code was derived from the finite element flow program FPM500 (Taylor and Brown, 1967). The program FPM500 performs flow modeling within saturated soil media. The major modifications introduced in order to implement the general flow equation (Eq. (3)) were based on the paper by Neuman (1973).

The mathematical development of the flow equation, built-in in the FLOW3D code, assumes that (i) flow is laminar and Darcian; (ii) inertial forces, velocity heads, temperature gradients and chemical concentration gradients are all negligible; (iii) soil is linearly elastic and isotropic; (iv) hydraulic properties are not affected by volume changes; (v) the air phase is continuous and always in connection with the constant, external atmospheric pressure. The program also considers that the hysteretic behaviour of the SWRC is negligible and, therefore, soil suction (ψ) is a single value function of volumetric water content (θ). The effect of soil compressibility on the storage of water under unsaturated conditions is quite small; therefore, the coefficient of specific storage (S_s) is disregarded.

The program FLOW3D was tested for various steady and unsteady state flow conditions and geometries. 1D steady-state state was simulated by prescribing constant pressure heads at the boundaries of an unsaturated soil profile. The results were compared to the exact solution. At the center of the soil layer, the difference in matric suction was less than 1%.

A 1D transient flow problem (Fig. 11), originally analyzed by Buchanan et al. (1980) with a finite difference model, was also simulated. The rainfall rate was adopted as being one-tenth of the saturated hydraulic conductivity, in order to assure infiltration without ponding, and an impervious condition was prescribed at the lower boundary. The reliability of the numerical results was evaluated by comparing the volume of infiltrating water through computations of changes in soil moisture (Fig. 11b). After 10 h of simulation, the phreatic level reached the soil surface and the assumption of continuous infiltration is no longer valid.

The 2D steady-state condition was simulated by prescribing pressure heads at the reservoir boundary of a homogeneous earth dam, with a horizontal drain at the toe. The dam foundation was considered impervious. In the unsaturated region, the soil moisture and hydraulic conductivity were adopted as being, respectively, one third and 0.01 of the corresponding saturated values. At the beginning of the numerical simulation pressure heads were constant and equal to 0.98 kPa. During the transient process, the wetting front moves towards the drain, until equilibrium is reached. The time interval needed to achieve the steady-state condition is dependent on hydraulic parameters. Once achieving this state,

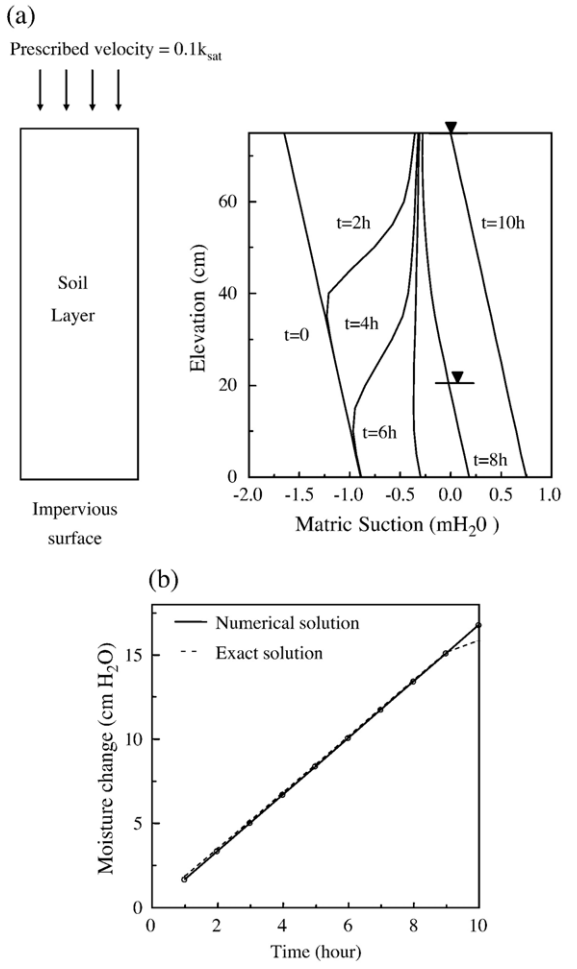

Fig. 11. 1D transient flow problem under a constant rainfall rate.

the phreatic line remains fixed, regardless further time intervals. A comparison with Kozeny's solution showed a good agreement.

The 3D transient flow condition was evaluated by simulating a 3D model experiment run by Akai et al. (1979), shown schematically in Fig. 12a. Inside the experimental box, a 50-cm-thick layer of sand was initially compacted. Before starting the experiment, the water table was located 7 cm above the base. The water level at one side of the impervious plate was raised instantaneously to the elevation of 47 cm and maintained at that position throughout the test. Fig. 12b shows numerical results at different time intervals. At the beginning of the infiltration process, the hydraulic gradients are higher, and they reduce when steady state is achieved. Fig. 12c compares the elevation of phreatic surfaces predicted by numerical simulation with the ones observed during the test, at section $z=100$ cm. At the beginning of the infiltration process, there is a time lag between the numerical result and the experimental response. This difference reduces with time and, after 120 min, the results show a good agreement.

4.2. Geometry and boundary conditions

The slope weathering profile is composed of an average 1-m-thick superficial mature residual soil, underlain by a saprolitic soil, with a thickness varying between 1 and 10 m. Topographic plants before and after the landslide, aerophotos taken in 1966 and 1975, and logging profiles were used to restore the original geometry of the slope. Fig. 13 shows the cross-section, corresponding to the center of the landslide.

The 3D slope profile prior to the slide was reconstituted by fitting seven 2D cross-sections. Fig. 14 shows the restored slope geometry and the nomenclature

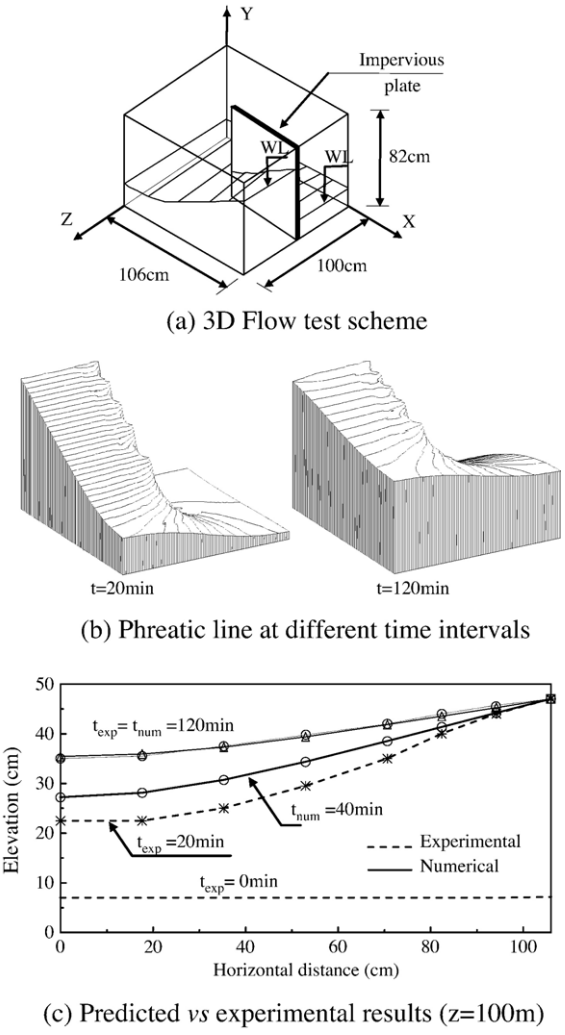

Fig. 12. Unsteady-state 3D transient flow problem.

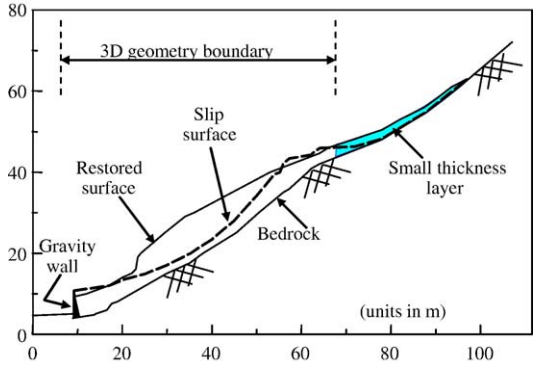

Fig. 13. Restored central cross-section of the slope.

adopted for the slope boundaries. The small thickness layer, located at the top of the slope (Fig. 13), was disregarded in the 3D analyses, in order to avoid excessive mesh discretization. Its effect was considered in the numerical analysis by prescribing specific boundary conditions at nodes located at the top boundary. These boundary conditions are further discussed in what follows. The 3D mesh was composed of 1820 elements and 2436 nodes.

The lateral boundaries were considered as impervious surfaces. This implies that flow directions were parallel to the lateral boundaries of the slope. This hypothesis may be questionable, since irregular geometries of soil profiles may generate lateral flow. Difficulties to reproduce flow regime within natural soils have, however, to be recognized. Obtaining accurate prediction of flow patterns is a difficult task and a number of simplifications are usually required.

The bottom of the slope was considered as an impervious surface. This is due to the assumption that clogging of internal drains occurred in the ancient gravity wall. This boundary condition is favourable to the development of positive pore pressures.

The embedded rock at the base of the slope was considered as an impervious surface, despite the existence of a transition layer between the sound rock and the saprolitic soil. This layer was identified as a highly fractured rock with varying thickness.

At the slope surface, daily rainfall events were simulated by prescribing flow velocities at the surface nodes. Flow velocities were computed according to daily rain amounts registered at the Lagoa pluviometric station, located 4 km away from the slope (Fig. 4a). The spatial variability of the rainfall amount was not significant. A pluviometric station installed on the roof of Building A, during the recovery works, indicated similar records to those from the Lagoa station, but with lower peak values of rain. It is worthwhile to note that, before failure, the slope surface was covered by dense vegetation. Thus, the actual volume of water that infiltrates at the soil surface would probably be smaller than the ones registered by the pluviometric stations.

4.3. Hydraulic parameters

The SWRC and the relationship between hydraulic conductivity and pressure head were inferred from experimental results.

The SWRC was introduced by considering linear intervals between each pair of experimental data points (Fig. 9). The small differences between drying and

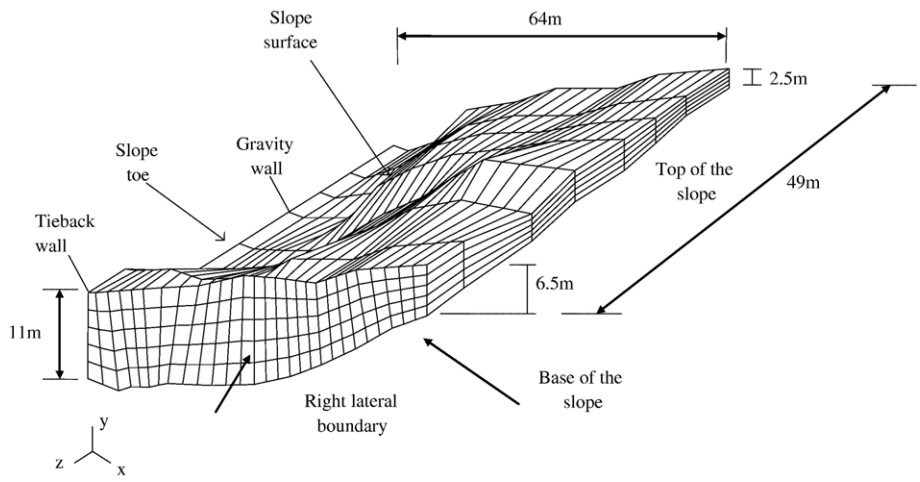

Fig. 14. Reconstituted 3D geometry and boundaries description.

wetting paths were disregarded and a single average curve was adopted.

Changes of the hydraulic conductivity with depth (Fig. 7) were incorporated in the analysis. Two layers were considered within the first 3 m of the soil profile. Below this depth, the hydraulic conductivity parameters were considered constant. The parameters are presented in Table 3 and, Fig. 15, shows the resultant relative hydraulic conductivity ($k_r = k/k_{sat}$) functions used, for each layer, in the present paper.

4.4. Time-dependent boundary conditions

The time dependent characteristic of the transient flow through unsaturated soil requires the knowledge of the antecedent distribution of matric suction (or soil moisture), previous to the simulation period. This information is very difficult to obtain since it would demand a previous monitoring of the slope or, eventually, a soil moisture database.

Flow modeling assumed null suction at the slope surface and a progressive increase of matric suction with depth. Below 2 m depth, the soil suction was taken as constant and equal to 200 kPa. These values were assumed by evaluating both the water content profile of the saprolitic soil (Fig. 7) and the soil–water retention curve (Fig. 9).

5. Flow pattern results

The main issue of this research was to understand how a rainstorm of medium magnitude could completely saturate the Lagoa slope and consequently induce a huge landslide. Different aspects were evaluated aiming at determining its influence on the hydrogeology of the slope.

5.1. Influence of rainfall intensity

The influence of rainfall intensity was initially evaluated by analysing flow pattern results considering a more intense rainfall that occurred few months before the landslide. In February 1988 (Fig. 4b), the accumulated rain amount was almost twice that registered in October and November (Fig. 4a).

Table 3
Hydraulic conductivity parameters

Depth (z) (m)	Saturated hydraulic conductivity (k_{sat}) (m/s)	Gardner's parameter (α) (m^{-1})
>1.5	1.7×10^{-5}	0.37
$1.5 \geq z \leq 3.0$	8.5×10^{-7}	0.88
z>3.0	1.2×10^{-5}	2.80

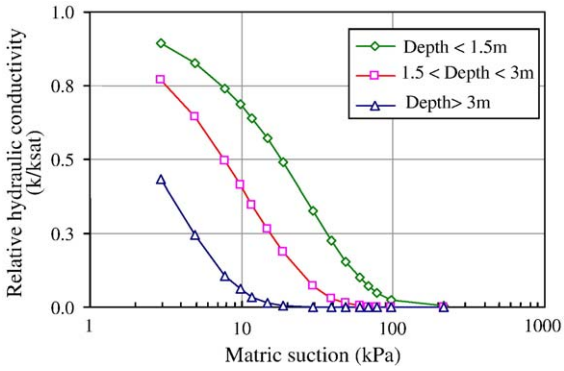

Fig. 15. Prescribed relative hydraulic conductivity curves.

The 3D slope geometry used in this analysis disregarded the small thickness layer (Fig. 13), located at the top of the slope above the failure region. All boundaries were considered impervious, except for the slope surface where the prescribed flow velocities at the nodes were equivalent to the rainfall registered in February.

After 21 days of simulation, beginning on February 3, the pressure head distribution, shown in Fig. 16, indicated slight changes in pressure head distributions, but no development of positive pore pressures within the soil slope. This water pressure condition was in disagreement to field observation, since failure surface had shown clear indication of being completely saturated. It was therefore concluded that rain infiltration would not be sufficient to produce significant pore-water changes.

5.2. Influence of the small thickness layer

The hypothesis of disregarding the small thickness layer (Fig. 13), located at the top of the slope, by assuming the upper surface as an impervious boundary, could have negatively influenced flow results.

The upper surface flow pattern was, therefore, re-evaluated by performing a 2D analysis considering the geometry of this varying thickness layer (Fig. 17). In this study, the initial distribution of matric suction was considered constant and equal to 10 kPa. The base of the layer was considered as an impervious surface. At the upper boundary, null pressure heads ($h_p = 0$) were prescribed at the nodes, due to its proximity to the rock that outcrops at the upper side of the landslide boundary. 17 days of numerical simulation revealed that rainfall intensities prior to November 2 (landslide day) could cause complete saturation of this small thickness layer. The assumption of an impervious surface at the upper

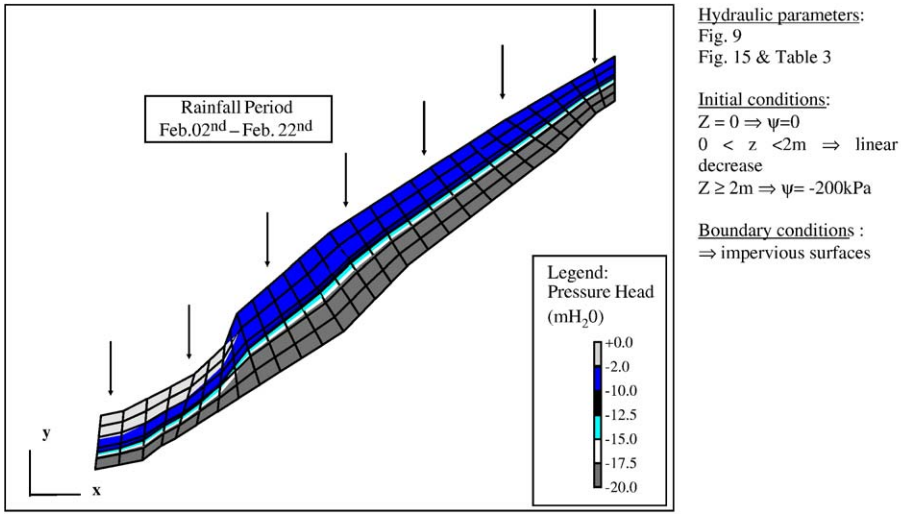

Fig. 16. 3D analysis: pressure head distribution in the central section of the slope, February 1988.

boundary of the slope was inadequate, even for lower rainfall intensities.

The effect of a saturation condition of the upper layer was introduced in the numerical analysis by prescribing hydrostatic pressure heads at the top boundary nodes of the 3D slope geometry. Fig. 18 presents the predicted pressure head distribution, at the central section of the slope, on the day of the Lagoa landslide. In this study, flow velocities prescribed at the nodes of the slope surface comprised 19 days of rain events, from October 19 to November 7. The results indicated positive pore pressure generation at the upper zone, mainly due to the progress of a saturation front, starting from the top of the slope. It is understandable that a water source has a strong influence on flow patterns. On the other hand, this result did not reproduce the saturation condition of the failure surface that was verified after the slide.

5.3. Influence of geometry changes after landslide

After the slope failure, the displacement of the soil mass modifies the flow pattern as the geometry changes. This influence was evaluated by performing a simplified 2D numerical simulation (Fig. 18). In this analysis, a high value of saturated hydraulic conductivity ($k_{sat}=1$) was used in contrast to the ones assigned to the

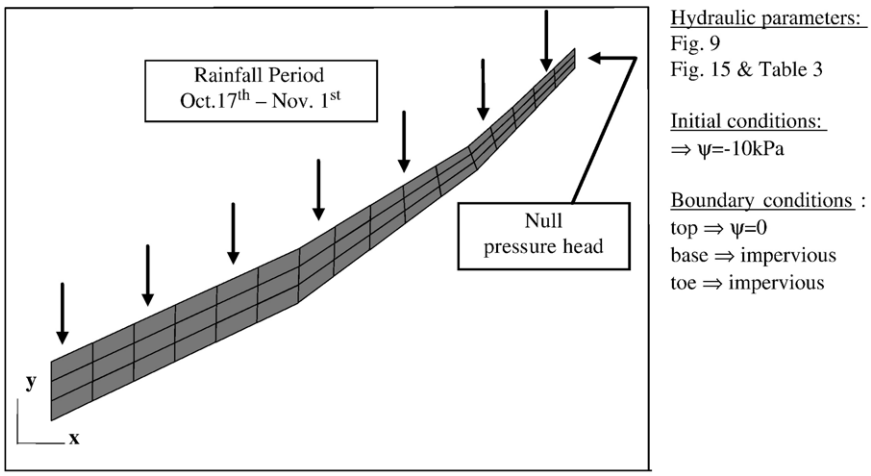

Fig. 17. 2D analysis: small thickness layer geometry and boundary conditions, November 1988.

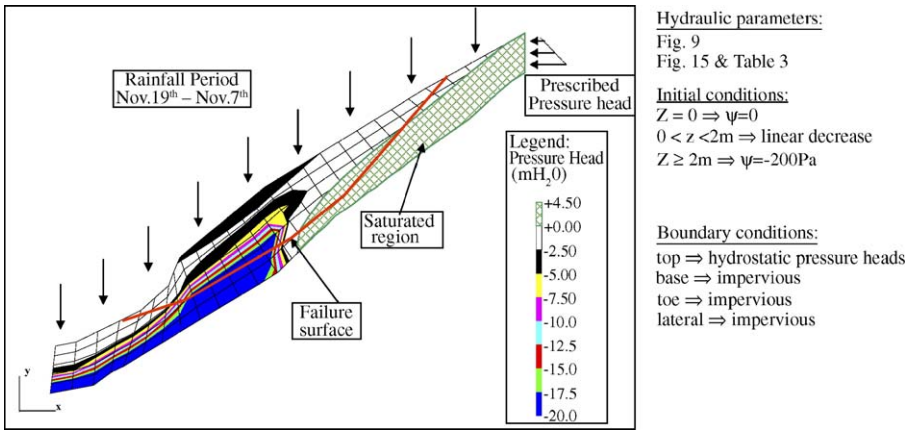

Fig. 18. 3D analysis: boundary conditions and pressure head distribution in the central section of the slope, November 1988.

remaining soil mass. Besides, null pressure heads were prescribed at the nodes located above failure surface. In this study, the initial distribution of pressure heads where equivalent to the ones predicted after 19 days of rain simulation, shown in Fig. 18. The remaining boundary conditions were identical to the previous ones. The results of the numerical analysis, presented in Fig. 19, revealed that a few hours were sufficient to nearly cause a saturation of the whole soil mass.

This scenario could be a feasible explanation for the saturation condition of the failure surface. On the other hand, it could not explain the landslide. Unexpected positive pore-water development might have occurred in order to reduce shear strength and cause the soil mass to fail.

5.4. Influence of the fractured rock transition

Field investigations indicated that the transition between the sound rock and the saprolitic soil consisted of a highly fractured rock with a thickness varying within 4–10 m. Water levels, measured by maxima piezometers, were restricted to this transition layer and were confined to a small area.

Field inspection, after landslide, revealed full obstruction of the crest channel adjacent to the landslide boundary. It is possible that the malfunction of the superficial drainage system induced favourable conditions to water infiltration and generated preferential flow paths through the fracture systems of the embedded rock. As a result, the highly fractured transition between the sound rock and saprolitic soil could have been saturated, and high hydraulic pressures could be originated at the base of the slope. It is a difficult task to predict and model such scenario, since a continuous monitoring of pressure heads at different points of the slope would be required. Nevertheless, the potential influence of the saturation of the fracture systems was roughly evaluated by prescribing positive pressure heads at 13 nodes, located along a transversal line of nodes at the base of the 3D mesh, as shown in Fig. 20. At each node, the magnitude of pressure head was equivalent to the vertical distance between the node coordinate and the highest point of the slope mesh. This simulation was

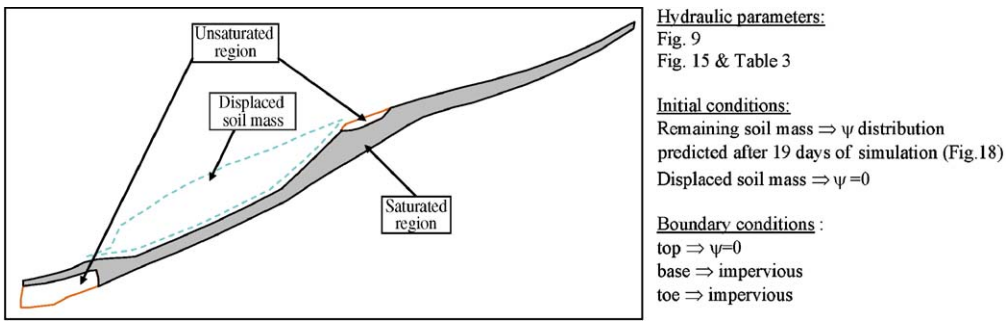

Fig. 19. 2D analysis: saturation distribution in the central section of the slope, 1 day after failure and disregarding displaced soil mass.

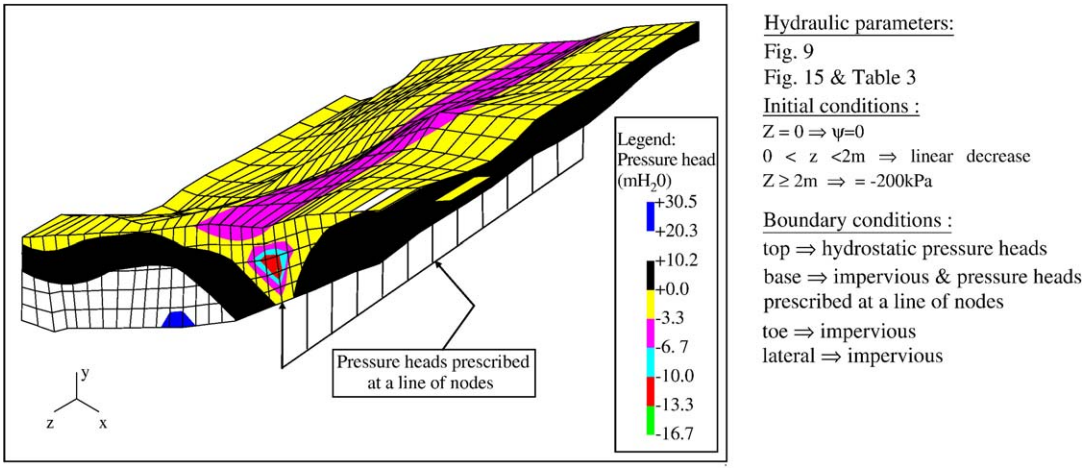

Fig. 20. 3D analysis: pressure head distribution with pressure heads prescribed at some nodes at base of the slope.

carried out for a time of approximately 6 days, from November 2 to November 7. Boundary conditions and antecedent soil suction were similar to the ones used in the previous analysis. The results, shown in Fig. 20, revealed the major influence of water sources when they occur at the base of the slope. Nearly the whole soil mass reached full saturation, with high levels of positive pore pressure having been achieved.

6. Conclusions

A comprehensive investigation was undertaken in an attempt to understand the hydraulic conditions that may have contributed to the deep-seated slide of the Lagoa slope, in Rio de Janeiro, Brazil. The landslide occurred in November 1988, after a rainfall period. However, the total rain amount recorded during this period was almost half of the magnitude of the one observed in February 1988.

Field observations taken on the following day and even 1 week after the slide indicated that the failure surface was fully saturated, with groundwater sprouting at its upper region, despite the nonexistence of groundwater within the soil mass. Further, there were indications that failure was triggered by positive pore-water pressure generation.

The slope consists of a varying thickness layer of unsaturated residual soil overlying a gneissic rock that outcropped at the upper and left sides of the landslide boundary. The transition between the sound rock and the saprolitic soil was densely fractured.

Despite the careful approach in determining geotechnical and hydrogeological parameters of the residual soils, numerical modeling of infiltration processes did not reproduce the saturation condition of the failure surface. The effect of geometry changes on the hydrogeological pattern of the slope, due to the displacement of the soil mass above the failure surface, on the hydrogeological pattern of the slope, was numerically evaluated and revealed that the internal redistribution of pore-water pressure could have contributed to the development of positive pore-pressures after the slide.

Several researchers pointed out the major role of the bedrock in generating high pore pressures. Hydrogeological modelling carried out by Dietrich et al. (1986) indicated that for many moderately sloping valleys, measured pore pressures could not be generated unless topographically driven by bedrock groundwater. Data from field investigation (Wilson, 1988) have also shown that the hydrologic response in moderately inclined slope was largely controlled by the groundwater circulation pattern in the bedrock, and these patterns resulted from large-scale topographic controls and small-scale heterogeneities in bedrock permeability. Vargas et al. (1990) compared flow-modeling results of geomorphological units that are typically found in tropical regions and pointed out the strong influence of boundary conditions, as shown in Fig. 21.

The hypothesis of water infiltration through the fractured transition between the young residual soil and the sound rock was roughly considered by prescribing pressure heads at a line of nodes at the base of the slope. The numerical modelling of this hypothetical boundary condition resulted in a quick development of pore-pressure within the soil mass. It is likely that the lack of maintenance of the superficial drainage system, adjacent to the slide area, may have contributed to these preferential flow paths.

The numerical analyses presented in this paper pointed out the complexity of flow modeling of rain infiltration through unsaturated residual soil slopes. It

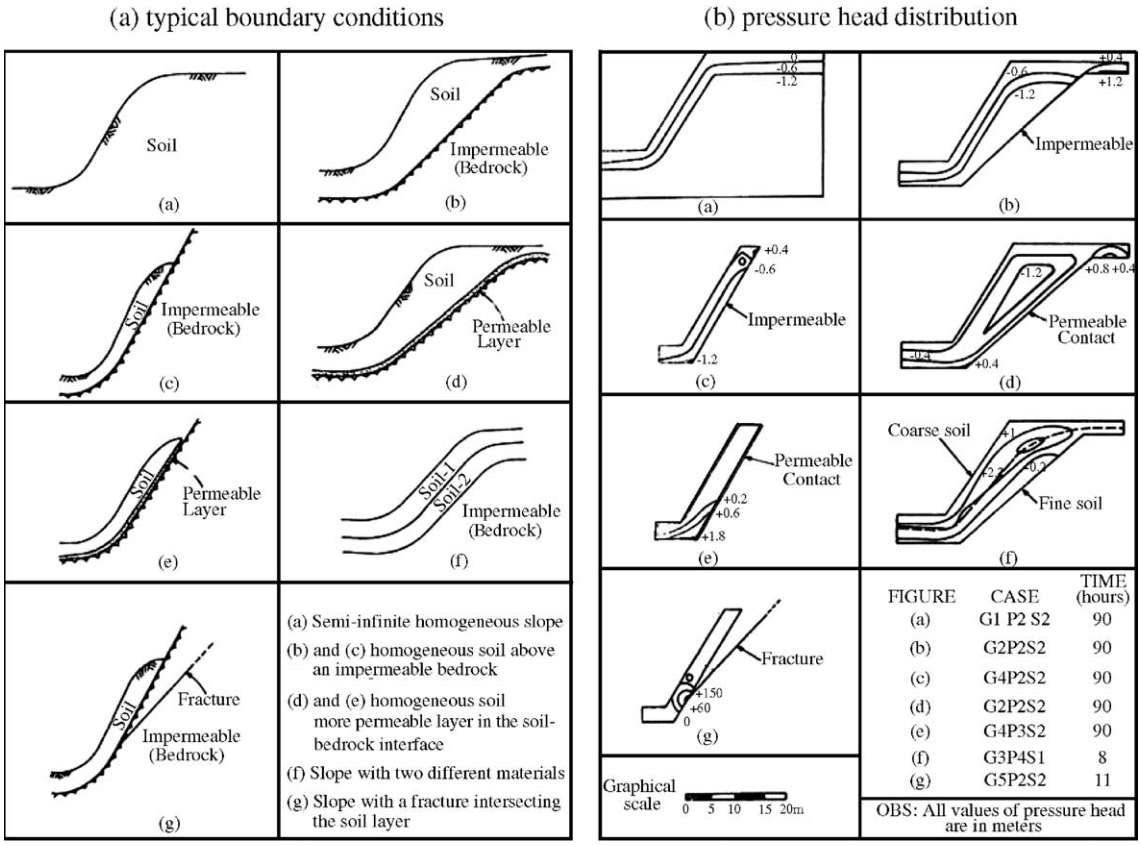

Fig. 21. Typical geomorphologic slopes and numerical results (Vargas et al., 1990).

essentially revealed that other flow mechanisms, besides rain infiltration just over the slope surface, played a major role on hydrological pattern of the Lagoa slope as it may develop preferential flow paths.

The engineering practice for predicting hydrological pattern of natural slopes rarely identifies the role that bedrock plays in generating high pore pressure. This is in part due to the difficulty and costs of installing an adequate number of deep piezometers to measure pressure head response in bedrock. In addition, unexpected preferential flow paths due to anisotropy of the hydraulic conductivity or due to flow through relic joints, that may be present in weathered profiles (Zhang et al., 2000), are hardly incorporated. Thus, the assumption of uniform porous media is the ordinary engineering design practice.

In order to define risk maps, a lot of research has been carried out in an attempt to quantify the magnitude of both rain intensity and duration that leads to slope instability of residual soil slopes. The strong influence of the antecedent moisture conditions on the hydrogeological response of unsaturated soil slopes to rain infiltration has already been recognized (e.g., Ng and Xi, 1998). However, besides the unexpected flow paths already pointed out, inefficient drainage systems or even leakage of buried pipes, which are not unusual, may also respond for some landslides (e.g., de Campos et al., 2006).

List of Symbols

α, a, n, m	equation parameters
C	volumetric water retention capacity
e	void ratio
G	specific gravity
h_p	pressure head
k	hydraulic conductivity
k_{sat}	saturated hydraulic conductivity
k_{ij}^s	hydraulic conductivity tensor at saturation
K_r	relative hydraulic conductivity
n	porosity
S	degree of saturation
S_s	coefficient of specific storage
ε	error criterion
ψ	matric suction
ψ_b	air entry or bubbling pressure
ψ_r	residual soil suction

γ_t in situ density
θ volumetric water content
θ_s saturated volumetric water content
θ_r residual volumetric water content
θ_i predicted volumetric water content
$\hat{\theta}_i$ measured volumetric water content
ω water content (in weight)
ω_{LL} liquid limit
ω_{LP} plasticity limit

Acknowledgements

The authors are grateful to the relevant contributions of Dr. P. Byrne, University of British Columbia, Canada. The authors acknowledge the International Development Research Center (IDRC), Canada, and the National Council for Research (CNPq), Brazil, for their financial support.

References

Akai, K., Ohnishi, Y., Nishigaki, M., 1979. Finite element analysis of three-dimensional flow in saturated-unsaturated soils. Proceedings of the 3rd Int. Conf. Numerical Methods in Geomechanics—Aachen, pp. 227–239. April.

Au, S.W.C., 1998. Rain-induced slope instability in Hong Kong. Engineering Geology 51 (1), 1–36.

Aubertin, M., Ricard, J.-F., Chapuis, R.P., 1998. A predictive model for the water retention curve: application to tailings from hard-rock mines. Canadian Geotechnical Journal 35, 55–69.

Brand, E.W., 1984. Landslides in south Asia. Proceedings of the 4th International Symposium on landslides, Toronto, vol. 1, pp. 17–59.

Brand, E.W., 1985. Geotechnical engineering in tropical residual soils. Proceedings of the 1st International Conference on Geomechanics in Tropical Lateritic and Saprolitic Soils, Brasılia, Brazil, vol. 3, pp. 23–100.

Brooks, R.H., Corey, A.T., 1964. Hydraulics Properties of Porous Media. Hydrol. Paper, vol. 3. Colorado State University.

Buchanan, P., Savigny, K.W., de Vries, J., 1980. A method for modeling water tables at debris avalanche headscarps. Journal of Hydrology 113, 61–68.

Costa Nunes, A.J., Fonseca, A.M.M.C., Hunt, R.E., 1979. Landslides of Brazil. Rockslides and Avalanches, Development in Geotechnical Engineering, vol. 2. Elsevier.

Costa Nunes, A.J., Couto Fonseca, A.M.M.C, de Couto Fonseca, M., Fernandes, C.E., Craizer, W., 1989. Intense rainstorm and ground slides. Proceedings of the 12th Int. Conf. Soil Mech. and Foundation Engineering, vol. 3, pp. 1627–1630.

de Campos, T.M.P., Moncada, M.P.H., Velloso, R.Q., Amaral, C.P., Vargas Jr., E.A., 2006. Evaluation of the Failure Mechanism of an Unsaturated Tropical Soil Slope. Geotechnical Special Publication, vol. 147. ASCE, pp. 485–496.

Dietrich, W.E., Wilson, C.J., Reneau, S.L., 1986. Hollows, colluvium, and landslides in soil mantled landscapes. In: Abrahams, A.D. (Ed.), Hillslope Processes. Allen & Unwin Ltd, pp. 361–368.

Elrick, D.E., Reynolds, W.D., Tan, K.A., 1989. Hydraulic conductivity measurements in the unsaturated zone using improved well analysis. Ground Water Monitoring Review 9, 184–193.

Fredlund, D.G., Xing, A., 1994. Equations for the soil water characteristic curve. Canadian Geotechnical Journal 31 (4), 521–532.

Freeze, R.A., Cherry, J.A., 1979. Groundwater. Prentice-Hall Inc., Englewood Cliffs, New Jersey.

Gardner, W.R., 1958. Some steady-state of the unsaturated moisture flow equation with application to evaporation from water table. Soil Science 85 (3), 228–232.

Gerscovich, D.M.S. 1994. Flow through saturated-unsaturated porous media: numerical modeling and slope stability studies of Rio de Janeiro natural slopes. DSc thesis, Civil Engineering Department, Catholic University of Rio de Janeiro (in Portuguese).

Gerscovich, D.M.S., Sayão, A.S.F.J., 2002. Evaluation of soil–water characteristic curves for soils from Brazil. unsaturated soils. In: Jucá, de Campos, Marinho (Eds.), A.A. Balkema, Lisse—3rd. International Conference on Unsaturated Soils, Recife, vol. 1, pp. 295–300.

Gerscovich, D.M.S., Guedes, M.N., Fonseca, E.T., 2004. Evaluation of soil–water characteristic curves for problems of unsaturated flow in soils from Brazil. Soils and Rocks—Latin-American Geotechnical Journal 27 (1), 57–68.

Gosh, R., 1980. Estimation soil moisture characteristics from mechanical properties of soils. Soil Science 130 (1), 60–63.

Hillel, D., 1971. Soil and Water: Physical Principles and Processes. Academic Press, Inc.

Jones, F.O., 1973. Lanslides of Rio de Janeiro and the Serra das Araras escarpment. Brazil. U.S. Geological Survey Paper, vol. 697.

Kim, J., Jeong, S., Park, S., Sharma, J., 2004. Influence of rainfall-induced wetting on the stability of slopes in weathered soils. Journal of Engineering Geology 75, 251–262.

Lumb, P., 1975. Slope failure in Hong Kong. Quarterly Journal Engineering Geology 8, 31–65.

Neuman, S.P., 1973. Saturated–unsaturated seepage by finite elements. Journal of Hydraulics Division. ASCE, vol. 99 (HY12), pp. 2233–2250.

Ng, C.W.W., Xi, Q., 1998. A numerical investigation of the stability of unsaturated soil slopes subjected to transient seepage. Computers and Geotechnics 22 (1), 1–28.

Rawls, W.J., Brakensiek, 1989. Estimation of soil water retention and hydraulic properties. In: Morel-Seytoux, H.J. (Ed.), Unsaturated Flow in Hydrologic Modeling: Theory and Practice. Kuwer Academic Publishers, pp. 275–300.

Reid, M.E., Nielsen, H.P., Dreiss, S.J., 1988. Hydrologic factors triggering a shallow hillslope failure. Bulletin of the Association of Engineering Geologists 25 (3), 349–361.

Reynolds, W.D., Elrick, D.E., 1987. A laboratory and numerical assessment of the Guelph permeameter method. Soil Science 144 (4), 282–292.

Taylor, M.E., Brown, C.B., 1967. Darcy's flow solution with free surface. Journal of Hydraulics Division. ASCE, vol. HY2, pp. 25–33.

van Genuchten, M.Th., 1980. A closed form equation for predicting the hydraulic conductivity of unsaturated soils. Proceedings of the Soil Science Society of America Journal, vol. 44(5), pp. 892–898.

Vanapalli, S.K., Fredlund, D.G., Pufahl, D.E., 1999. The influence of soil structure and stress history on the soil–water characteristics of a compacted till. Geotechnique 49, 143–159.

Vargas, M., 1971. Effect of rainfall and ground water levels. Proceedings of the 4th Pan American. Conf. Soil Mech. and Foundation Engineering, vol. 3, pp. 138–141.

Vargas Jr., E.A., Velloso, R.C., de Campos, T.M.P., Costa Filho, L. M., 1990. Saturated–unsaturated analysis of water flow in slopes of Rio de Janeiro, Brazil. Computers and Geotechnics 10 (3), 247–261.

Vaughan, P.R., 1985. Mechanical and hydraulic properties of in situ residual soils. Proceedings of the 1st International Conference on Geomechanics in Tropical Lateritic and Saprolitic Soils, Brasılia, vol. 3, pp. 231–263.

Wang, G., Sassa, K., 2003. Pore-pressure generation and movement of rainfall induced landslides: effect of grain size and fine-particle content. Engineering Geology 69, 109–125.

Wilson, C.J. 1988. Runoff and pore pressures in hollows. PhD Thesis, California University, Berkeley.

Wolle, C.M., Hachich, W., 1989. Rain-induced landslides in south-eastern Brazil. Proceedings of the 12th Int. Conf. Soil Mech. and Foundation Engineering, vol. 3, pp. 1639–1644.

Zhang, J., Jiao, J.J., Yang, J., 2000. In situ infiltration studies at a hillside in Hubei Province, China. Engineering Geology 57, 31–38.